# Fabrication, characterization, and application of polyaniline/Ni(II) metal-organic frameworks nanocomposite as a supercapacitor electrode material

**Zeinab Ansari-Asl** ( z.ansari@scu.ac.ir )
Shahid Chamran University of Ahvaz
**Amin Shiralizadeh Dezfuli**
Iran University of Medical Sciences (IUMS)

**Research Article**

**Keywords:** Nanocomposite, Polyaniline, Conductive polymer, Metal-organic framework, Supercapacitor

**Posted Date:** May 28th, 2021

**DOI:** https://doi.org/10.21203/rs.3.rs-561933/v1

# Abstract

Metal-organic frameworks (MOFs), owing to their tunable porosity, high surface area, and diversity were investigated as potential supercapacitor materials. PANI/Ni-MOF, a nanocomposite of Ni-MOF and polyaniline (PANI), was fabricated by *in situ* solvothermal synthesis of Ni-MOF in the presence of the as-obtained PANI. The prepared products were studied using FT-IR, PXRD, SEM, and EDS-mapping techniques. EDS-mapping results exhibited the uniform dispersion of Ni-MOF into the polymeric matrix. Electrochemical properties of the pure Ni-MOF and PANI/Ni-MOF were investigated through CV (cyclic voltammetry), GCD (galvanostatic charge/discharge), and EIS (electrochemical impedance spectroscopy) methods in a three-electrode system. The as-fabricated PANI/Ni-MOF nanocomposite exhibited outstanding electrochemical performance owing to the synergistic effects of PANI with proper conductivity and the Ni-MOF's porous structure, obtaining an excellent specific capacitance of 601 F $g^{-1}$ at 1 A $g^{-1}$. Additionally, this supercapacitor material showed a remarkable cycle life after 5000 charge/discharge test, 99.5 % retention of its specific capacitance. These excellent properties would make PANI/Ni-MOF nanocomposite as a proper candidate for supercapacitor electrode material. .


# 1. Introduction

Todays, wind and solar energies have attracted much attention as renewable sources to overcome the fossil fuel challenges. Nevertheless, for the storage and application of these energies, using some electrochemical devices is essential [1,2]. Supercapacitors owing to their long cycle life, high power density, and great reversibility, are the most investigated energy storage devices. Based on the charge/discharge mechanisms, these devices are divided into pseudocapacitors and electrical double-layer capacitors (EDLCs) [3–5].

Recently, MOF-based materials have been investigated as supercapacitor electrode materials. These structures have outstanding features such as high porosity, versatility, and high surface area. Owing to their controllable pore size, tunable pore structures, and high porosity, these structures can facilitate ionic diffusion and offer increased active sites [6,7]. For instance, Yan *et al*. investigated the MIL-47, rod-like vanadium metal-organic frameworks, as an electrode material. This electrode exhibited a specific capacitance of 572.1 F $g^{-1}$ at current densities of 0.5 A $g^{-1}$ [8]. In another study, Lee *et al.* reported a specific capacitance around 206.8 F $g^{-1}$ for the doctor-bladed Co-MOF film as a supercapacitor electrode [9].

Nevertheless, the low electrical conductivity and fragile nature greatly hinder the potential of MOFs for high energy storage. Compare to pure MOFs, their nanocomposites provided proper performance to the storage of energies [10,11]. Conducting polymer-based nanocomposites of various MOFs have exhibited proper properties as components of supercapacitor materials [12,13]. PANI is one of the most used conductive polymer that exhibited valuable characteristics such as good electrical conductivity and reversibility [14,15]. For example, the ZnO@MOF@PANI core-shell nanocomposite exhibited a high

specific capacitance around 340.7 $Fg^{-1}$ at 1 A $g^{-1}$ [16]. In another study, Bao *et al.* have reported a specific capacitance of 372 F $g^{-1}$ at 0.1 A $g^{-1}$ for rGO/Zn-MOF@PANI composite [17].

In this study, the PANI/Ni-MOF nanocomposite was prepared by *in situ* synthesis of Ni-MOF in the presence of the as-prepared PANI, in which Ni-MOFs were uniformly distributed into the PANI matrix. The prepared compounds were investigated by FT-IR, PXRD, SEM, and EDS-mapping spectroscopy. To confirm the potential of the PANI/Ni-MOF as a working electrode material, the electrochemical performance of this sample was studied in a three-electrode set-up in KOH (6 M) as an electrolyte. The as-fabricated PANI/Ni-MOF nanocomposite showed higher specific capacitance (601 F $g^{-1}$ at 1 A $g^{-1}$) than the pristine Ni-MOF. Additionally, this electrode material exhibits outstanding cycling stability around 99.5 % after 5000 cycles.

# 2. Experimental

## 2.1. Materials and methods

Nickel(II) nitrate hexahydrate, dimethylformamide (DMF), ethanol (EtOH), ammonium persulfate (APS), polytetrafluoroethylene (PTFE), and acetylene black were obtained from Merck company. Aniline and 1,3,5-benzenetricarboxylic acid ($H_3BTC$) were purchased from Aldrich company. All reagents were applied without any further modification. Woven 304 stainless steel grid was purchased from Yangzhou Jinrun Mesh Belt Manufacturing Company. The chemical composition of the as-fabricated materials was investigated via FT-IR (Fourier transform infrared), BOMEM MB102 spectrophotometer. The microcrystalline structure of the materials was identified by powder X-ray diffraction (PXRD) patterns using an X'Pert Pro diffractometer (CuKα radiation, λ = 1.5405 Å). The morphological studies were conducted by field emission scanning electron microscopy (FESEM-*KYKY-EM3200*) at 15 kV.

## 2.2. Synthesis of Ni-MOF

In a typical preparation, 2.90 g (10 mmol) of $Ni(NO_3)_2.6H_2O$ and 1.05 g (5 mmol) of $H_3BTC$ were dissolved in 60 mL of EtOH:$H_2O$:DMF (volume ratio 1:1:1). The obtained solution was transferred to a stainless steel autoclave (Teflon-lined stainless steel) and heated at 85 ℃ for 20 h. After cooling the autoclave to room temperature, the obtained Ni-MOF crystals were filtered, washed with distilled water and ethanol, and dried at 60 ℃ for 24 h.

## 2.3. Synthesis of polyaniline (PANI)

PANI was prepared as mentioned in the literature [18]. 4.5 mL of PANI monomer was added to 100 mL of distilled water and stirred in an ice-bath for 30 min. Then, 25 mL of $H_2SO_4$ (2 M) was added. After that, 50 mL ammonium persulfate (0.25 M) was added into above-mentioned solution slowly for 1 h. The mixture was stirred for 4 h in an ice bath and aged for 24 h at room temperature. Then, the PANI was centrifuged and washed with distilled water and ethanol, and dried at 60℃ for 12 h.

## 2.4. Synthesis of PANI/Ni-MOF nanocomposite

0.10 g of PANI was added to 12 mL of EtOH:$H_2O$:DMF (volume ratio 1:1:1) and sonicated for 1 h. $H_3BTC$ (0.42 g, 2 mmol) and $Ni(NO_3)_2.6H_2O$ (1.17 g, 4 mmol) were completely dissolved in 12 mL of EtOH:$H_2O$:DMF (volume ratio 1:1:1). Then, the obtained PANI suspension was mixed with the solution of nickel salt and organic linker by sonication; the resulting well-dispersed mixture was transferred to the stainless steel autoclave. The reaction was carried out at 85 ℃ for 20. Finally, the autoclave was cooled to room temperature and the as-fabricated PANI/Ni-MOF nanocomposite was centrifuged, washed with distilled water and ethanol, and dried at 60 ℃ for 24.

### 2.5. Electrochemical Measurement

To prepare the working electrode, acetylene black (25%), polytetrafluoroethylene (PTFE) (5%), and Ni-MOF or PANI/Ni-MOF nanocomposite (70%) were mixed in a negligible volume of ethanol. Then, the obtained paste was coated on the stainless steel grid (1 cm×0.5 cm). The as-obtained electrode was pressed and dried 60 ℃ for 5 h. A three-electrode system was used to test the electrochemical performance of the Ni-MOF and PANI/Ni-MOF nanocomposite, on the Autolab 302N, Eco Chemie B. V. The as-obtained electrode, graphite rod, and Ag/AgCl were used as the working electrode, counter electrode, and reference electrode, respectively. The CV (within -0.5 to +0.5 V), GCD, and EIS measurements were conducted in KOH solution (6 M) at ambient conditions.

## 3. Results And Discussion

### 3.1. Structure characterization

In this project, Ni-MOFs were synthesis in the presence of the as-fabricated PANI via the solvothermal method. The obtained compounds were characterized using FTIR, PXRD, SEM, and EDS-mapping spectroscopy. Electrochemical properties of the pure Ni-MOF and its PANI nanocomposite electrodes were studied in a three-electrode cell in KOH (6 M) electrolyte with an Ag/AgCl reference electrode and a graphite counter electrode through CV, GCD, and EIS studies.

Figure **1** shows FT-IR spectra of Ni-MOF, PANI, and PANI/Ni-MOF nanocomposite. For Ni-MOF, the characteristic absorption peaks at 1605 $cm^{-1}$ and 1516 $cm^{-1}$ are ascribed to the asymmetric vibrations of the carboxylate groups ($COO^-$) of benzenetricarboxylate (BTC) ligands, while the bands at 1420 $cm^{-1}$ and 1366 $cm^{-1}$ are corresponded to the symmetric vibrations of this group. The bands at 1107 $cm^{-1}$ and 915 $cm^{-1}$ are related to the and , respectively, showing the coordination of Ni(II) to DMF [19–21]. In the FT-IR spectra of the PANI, the distinct absorption bands at 1566 $cm^{-1}$ and 1470 $cm^{-1}$ are associated with the C=C vibrations. The characteristic peaks at 1102 $cm^{-1}$ and 1204 $cm^{-1}$ are attributed to the C-H stretching of benzenoid and quinoid rings, respectively. Furthermore, the FT-IR spectrum of the PANI shows a peak at 1302 $cm^{-1}$ correspond to the C-N stretching [22,23]. The out-of-plane bending vibration of the C-H appeared at 798 $cm^{-1}$. As can be seen, the PANI/Ni-MOF nanocomposite exhibits the same functional groups with pristine PANI and Ni-MOF.

The microstructures of the Ni-MOF, PANI, and PANI/Ni-MOF nanocomposite are given in Figure **2**. The sharp diffraction peaks of Ni-MOF indicating its crystalline structure [24]. For PANI, the prominent diffraction peaks at 2 about 22º and 27º corresponds to its amorphous structure [23]. The PXRD pattern of the PANI/Ni-MOF showed a similar pattern to the PANI and Ni-MOF, indicated their presence into the final nanocomposite.

The morphological features of PANI and PANI/Ni-MOF composite were studied by SEM. Figure **3a** and **3b** confirm the semi-spherical morphology of the PANI and PANI/Ni-MOF with a diameter of 140 nm and 220 nm, respectively. The presence of Ni element in the PANI/Ni-MOF nanocomposite was confirmed by the EDS-mapping technique as given in Figure **3c**, which confirms the homogenous distribution of the Ni-MOF into the PANI matrix.

### 3.2. Electrochemical characterization

The electrochemical properties of Ni-MOF and PANI/Ni-MOF nanocomposite as an electrode were investigated by a three-electrode cell in KOH (6 M) through cyclic voltammetry, galvanostatic charge/discharge, and impedance methods. The Ag/AgCl, graphite rod, and Ni-MOF or PANI/Ni-MOF nanocomposite were applied as a reference, counter electrode, and working electrode, respectively. The CV curves in the potential range of -0.5 to +0.5 mV were given in Figure **4**. Deviation of rectangular shape and the presence of obviously reduction/oxidation peaks corresponds to the pseudocapacitance characteristic of the as-obtained electrodes [25,26]. Additionally, when the scan rates were increased, the same shape of CV curves can be observed. The larger CV area for PANI/Ni-MOF nanocomposite compared to the pure Ni-MOF can be attributed to the synergic effects of the pristine component [27,28].

As shown in Figure **4a**, **b**, the CV curves of Ni-MOF and PANI/Ni-MOF nanocomposite were investigated at various scan rates for further study of their electrochemical performance. The CV curves of the Ni-MOF exhibit symmetric structure at a low scanning speed, owing to the reversible redox process [29,30]. By increasing the scan rates from 5 to 100 $mVs^{-1}$, the cathodic and anodic peaks shifted to more negative and positive potential, respectively, owing to the internal resistance and polarization process [31,32]. The CV curves of the Ni-MOF and PANI/Ni-MOF nanocomposite were compared at 50 mV $s^{-1}$ (**4c**). The CV curve of the PANI/Ni-MOF has a greater area than the pristine Ni-MOF, confirming higher specific capacitance for this nanocomposite. Equation **1** can be used to determine the specific capacitance of the as-prepared electrodes [33,34]

$$C = \frac{Q}{V} = \int \frac{idt}{\Delta V} \qquad \text{Equation 1}$$

Where i, V, and t are the applied current, the voltage change, and time, respectively.

The specific capacitances of the Ni-MOF and PANI/Ni-MOF nanocomposite electrodes are given in Figure **5d**, at various scan rates from 5 to 200 mV $s^{-1}$. The Ni-MOF in the absence of polyaniline possesses 348 F

$g^{-1}$, while the specific capacitance was improved to 533 F $g^{-1}$ for PANI/Ni-MOF nanocomposite at 50 mV $s^{-1}$, ascribing to the synergistic interaction of polyaniline and Ni-MOF [18,35].

**Figure 4.** CV curves of (a) Ni-MOF and (b) PANI/Ni-MOF nanocomposite electrodes at different scan rates, (c) CV curves of Ni-MOF and PANI/Ni-MOF composite electrodes at 50 mV $s^{-1}$ scan rate in 6 M KOH electrolyte in the potential range from -0.5 to 0.5 V, and (d) alteration of calculated specific capacitance as a function of scan rate.

The GCD study was also employed to prove the electrochemical performance of the as-prepared compounds (Figure **5**). The symmetrical charge/discharge curves in GCD, well-adjusted with the CV results, indicating reversible redox reactions for the as-obtained electrodes. The faradic redox mechanisms for the tested electrodes can be distinguished by the GCD curves with gently sloping potential shape [36,37]. Furthermore, the PANI/Ni-MOF electrode has a longer discharge time that suggests higher specific capacitance than the pure Ni-MOF. The specific capacitance at different current densities was calculated from GCD curves using Equation **2**, and the obtained results are given in Figure **5d**, it can be seen that PANI/Ni-MOF nanocomposite has more specific capacitance than the pure Ni-MOF [38,39]. The obtained capacitance from GCD curves, in agreement with cyclic voltammetry results, confirmed the enhancement of the capacitance of PANI/Ni-MOF nanocomposite owing to the PANI conductivity.

$$C\ (F) = \frac{i}{\Delta V/\Delta t}$$ Equation **2**

Where C = specific capacitance, i = applied current, $\Delta V/\Delta t$ = slope of discharge curve.

Furthermore, the symmetrical characteristic of charge/discharge curves shows the proper electrochemical reversibility [40,41]. The faradic processes and pseudocapacitance characteristic of the as-prepared electrodes can further be verified by their nonlinear discharge curves [42]. Generally, the high porosity of MOFs can increase active sites that results in more redox reactions and better capacitance property [43].

The Ni-MOF and PANI/Ni-MOF nanocomposite electrodes were investigated for cycling performance by studying at 100 mV $s^{-1}$ for 5000 times (Figure **6**). The PANI/Ni-MOF nanocomposite shows better retention, 99.5 %, after 5000 cycles. Good cycle stability of active material is considered an essential characteristic for application as a supercapacitor electrode. The oxidation-reduction reactions and hence reduction of the active material amount is the main reason to decrease its specific capacitance during the cycle stability investigation [44].

EIS study is usually conducted to investigate the electrode's respond to frequencies. As exhibited in Figure **7**, the Nyquist plot can be divided into the intercepting of the x-axis and a straight line in the high and low-frequency domains, respectively [45]. The internal resistance of the electrodes ($R_s$) can be determined by

the intersection of the EIS curve with the x-axis at the high-frequency range. This parameter consists of the contact resistance between the active material and electrolyte, the internal resistance of the active electrolyte, and the electrolyte ion resistance. The smaller $R_s$ ascribed to the greater electrical conductivity of the sample [46]. The Ni-MOF and PANI/Ni-MOF nanocomposite showed the Rs values of 0.23 Ohm and 0.21 Ohm, respectively, showing that PANI-based nanocomposite of the Ni-MOF can decrease the internal resistance of the electrode. In addition, the PANI/Ni-MOF has higher electrical and ionic conductivity based on its lower Rs value. The $R_{ct}$ (charge transfer resistance) due to the faradic reactions can be determined from the semicircle diameter in the EIS curves. The Ni-MOF and PANI/Ni-MOF nanocomposite exhibit the $R_{ct}$ of 3 Ohm and 2.2 Ohm, respectively. The lower $R_{ct}$ of PANI/Ni-MOF nanocomposite compare to the Ni-MOF is corresponded to the high conductivity and better charge transfer kinetics of the PANI [47,48]. Additionally, owing to the synergistic effects between PANI and Ni-MOF, the PANI/Ni-MOF nanocomposite exhibits a steeper straight line than pure Ni-MOF that confirms its better capacitance.

# 4. Conclusion

The PANI-based nanocomposite of Ni-MOF, PANI/Ni-MOF, was fabricated by *in situ* synthesis of Ni-MOF in the presence of PANI and studied by various techniques to determine its functional groups and morphology. The as-fabricated nanocomposite showed a spherical morphology with a diameter around 220 nm. The electrochemical performance of the Ni-MOF and PANI/Ni-MOF nanocomposite were studied in KOH (6 M) electrolyte using a standard three-electrode system. The enhanced electrochemical performance was observed for the PANI/Ni-MOF nanocomposite, a specific capacitance around 601 F $g^{-1}$ at 1 A $g^{-1}$ owing to the rich nitrogen content, porous and amorphous structure of nanocomposite that can facilitate ion and electron transfer. Additionally, PANI/Ni-MOF nanocomposite exhibited a small solution resistance and charge transfer resistance. The PANI/Ni-MOF nanocomposite and Ni-MOF showed capacitance retention around 99.5 % and 94 % after 5000 cycles, respectively. Therefore, the fabrication of Ni-MOF nanocomposite with the conductive polyaniline polymer matrix can be considered a proper strategy to enhance the specific capacitance and cycle life of the final electrode materials. The obtained results highlight the applications of PANI/Ni-MOF nanocomposite as promising supercapacitor electrode material.

# Declarations


### Acknowledgements

This study was financially supported by Shahid Chamran University of Ahvaz (Grant No.: SCU.SC98.29011).


### Declaration of competing interest

There are no conflicts to declare.

# References

[1] M.J. Burke, J.C. Stephens, Energy Res. Soc. Sci. 35, 78 (2018) https://doi.org/10.1016/j.erss.2017.10.018.

[2] W. Miao, J. Wang, J. Liu, Y. Zhang, Adv. Mater. Interfaces. 5, 1800167 (2018) https://doi.org/10.1002/admi.201800167.

[3] P. Wang, X. Du, T. Chen, X. Hao, A. Abudula, K. Tang, G. Guan, Electrochim. Acta. 306, 35 (2019) https://doi.org/10.1016/j.electacta.2019.03.106.

[4] J. Jose, S.P. Jose, T. Prasankumar, S. Shaji, S. Pillai, S.P. B, J. Alloys Compd. 855, 157481 (2021) https://doi.org/10.1016/j.jallcom.2020.157481.

[5] M. Naushad, T. Ahamad, M. Ubaidullah, J. Ahmed, A.A. Ghafar, K.M. Al-Sheetan, P. Arunachalam, J. King Saud Univ. Sci. 33, 101252 (2021) https://doi.org/10.1016/j.jksus.2020.101252.

[6] S. Xiong, S. Jiang, J. Wang, H. Lin, M. Lin, S. Weng, S. Liu, Y. Jiao, Y. Xu, J. Chen, Electrochim. Acta. 340, 135956 (2020) https://doi.org/10.1016/j.electacta.2020.135956.

[7] Q. Li, H. Guo, R. Xue, M. Wang, M. Xu, W. Yang, J. Zhang, W. Yang, Int. J. Hydrogen Energy. 45, 20820 (2020) https://doi.org/10.1016/j.ijhydene.2020.05.143.

[8] Y. Yan, Y. Luo, J. Ma, B. Li, H. Xue, H. Pang, Small. 14, 1801815 (2018) https://doi.org/10.1002/smll.201801815.

[9] D.Y. Lee, S.J. Yoon, N.K. Shrestha, S.-H. Lee, H. Ahn, S.-H. Han, Microporous Mesoporous Mater. 153, 163 (2012) https://doi.org/10.1016/j.micromeso.2011.12.040.

[10] W. Zheng, S. Sun, Y. Xu, R. Yu, H. Li, ChemElectroChem. 6, 3375 (2019) https://doi.org/10.1002/celc.201900687.

[11] T. Yue, C. Xia, X. Liu, Z. Wang, K. Qi, B.Y. Xia, Chem. Electro. Chem. 8, 1021 (2021) https://doi.org/10.1002/celc.202001418.

[12] K. Qi, R. Hou, S. Zaman, Y. Qiu, B.Y. Xia, H. Duan, ACS Appl. Mater. Interfaces. 10, 18021 (2018) https://doi.org/10.1021/acsami.8b05802.

[13] A. Ehsani, M. Bigdeloo, F. Assefi, M. Kiamehr, R. Alizadeh, Inorg. Chem. Commun. 115, 107885 (2020) https://doi.org/10.1016/j.inoche.2020.107885.

[14] N. K, C.S. Rout, RSC Adv. 11, 5659 (2021) https://doi.org/10.1039/D0RA07800J.

[15] S.I. Abd Razak, I.F. Wahab, F. Fadil, F.N. Dahli, A.Z. Md Khudzari, H. Adeli, Adv. Mater. Sci. Eng. 2015, 356286 (2015) https://doi.org/10.1155/2015/356286.

[16] C. Zhu, Y. He, Y. Liu, N. Kazantseva, P. Saha, Q. Cheng, J. Energy Chem. 35, 124 (2019) https://doi.org/10.1016/j.jechem.2018.11.006.

[17] L. Quoc Bao, T.-H. Nguyen, H. Fei, I. Sapurina, F.A. Ngwabebhoh, C. Bubulinca, L. Munster, E.D. Bergerová, A. Lengalova, H. Jiang, T. Trong Dao, N. Bugarova, M. Omastova, N.E. Kazantseva, P. Saha, Electrochim. Acta. 367, 137563 (2021). https://doi.org/10.1016/j.electacta.2020.137563.

[18] S. Guo, Y. Zhu, Y. Yan, Y. Min, J. Fan, Q. Xu, H. Yun, J. Power Sources. 316, 176 (2016) https://doi.org/10.1016/j.jpowsour.2016.03.040.

[19] H. Tan, C. Liu, Y. Yan, J. Wu, J. Wuhan Univ. Technol. Sci. Ed. 30, 71 (2015) https://doi.org/10.1007/s11595-015-1103-z.

[20] F. Israr, D. Chun, Y. Kim, D.K. Kim, Ultrason. Sonochem. 31, 93 (2016) https://doi.org/10.1016/j.ultsonch.2015.12.007.

[21] Nirmal, K. Sharma, Poonam, S.K. Tripathi, AIP Conf. Proc. 2265, 30617 (2020) https://doi.org/10.1063/5.0017162.

[22] C.S. Zhang, L. Yang, Magn. Magn. Mater. 324, 1469 (2012) https://doi.org/10.1016/j.jmmm.2011.09.036.

[23] F.S. Omar, A. Numan, N. Duraisamy, M.M. Ramly, R. K., R. S., Electrochim. Acta. 227, 41 (2017) https://doi.org/10.1016/j.electacta.2017.01.006.

[24] D. Wang, W. Ni, H. Pang, Q. Lu, Z. Huang, J. Zhao, Electrochim. Acta. 55, 6830 (2010) https://doi.org/10.1016/j.electacta.2010.05.084.

[25] L. Li, H. Bi, S. Gai, F. He, P. Gao, Y. Dai, X. Zhang, D. Yang, M. Zhang, P. Yang, Sci. Rep. 7, 43116 (2017) https://doi.org/10.1038/srep43116.

[26] O. Okhay, A. Tkach, Nanomater. 11, 1240 (2021). https://doi.org/10.3390/nano11051240.

[27] D. Wang, Y. Zhang, L. Yang, G. Fan, Y. Lin, F. Li, J. Mater. Sci. Mater. Electron. 31, 6467 (2020) https://doi.org/10.1007/s10854-020-03202-3.

[28] H. Wang, J. Lin, Z.X. Shen, J. Sci. Adv. Mater. Devices. 1, 225 (2016) https://doi.org/10.1016/j.jsamd.2016.08.001.

[29] H. Li, F. Musharavati, J. Sun, F. Jaber, E. Zalnezhad, K.N. Hui, K.S. Hui, J. Electrochem. Soc. 165, 407 (2018) https://doi.org/10.1149/2.0111803jes.

[30] G. Liu, H. Zhang, J. Li, Y. Liu, M. Wang, J. Mater. Sci. 54, 9666 (2019) https://doi.org/10.1007/s10853-019-03536-2.

[31] M. Sajjad, Y. Khan, CrystEngComm. 23, 2869 (2021) https://doi.org/10.1039/D1CE00073J.

[32] G. Babu, K. Ababtain, K.Y.S. Ng, L.M.R. Arava, Sci. Rep. 5, 8763 (2015) https://doi.org/10.1038/srep08763.

[33] P. Tang, Y. Zhao, C. Xu, K. Ni, J. Solid State Electrochem. 17, 1701 (2013) https://doi.org/10.1007/s10008-013-2021-7.

[34] Z. Neisi, Z. Ansari-Asl, A.S. Dezfuli, J. Inorg. Organomet. Polym. Mater. 29, 1838 (2019) https://doi.org/10.1007/s10904-019-01145-9.

[35] Z. Li, L. Gong, Mater. 13, 548 (2020). https://doi.org/10.3390/ma13030548.

[36] R. Jia, Y. Wu, G. Zan, D. Liu, Mater. Sci. Mater. Electron. 28, 2366 (2017) https://doi.org/10.1007/s10854-016-5805-6.

[37] A. Bahaa, J. Balamurugan, N.H. Kim, J.H. Lee, J. Mater. Chem. A. 7, 8620 (2019) https://doi.org/10.1039/C9TA00265K.

[38] Y. Jiao, G. Chen, D. Chen, J. Pei, Y. Hu, J. Mater. Chem. A. 5, 23744 (2017) https://doi.org/10.1039/C7TA07464F.

[39] T.P. Mofokeng, A.K. Ipadeola, Z.N. Tetana, K.I. Ozoemena, ACS Omega. 5, 20461 (2020) https://doi.org/10.1021/acsomega.0c02563.

[40] J. Cherusseri, D. Pandey, J. Thomas, Batter. Supercaps. 3, 860 (2020) https://doi.org/10.1002/batt.201900230.

[41] F. Cai, R. Sun, Y. Kang, H. Chen, M. Chen, Q. Li, RSC Adv. 5, 23073 (2015) https://doi.org/10.1039/C5RA02058A.

[42] C. Dong, Y. Wang, J. Xu, G. Cheng, W. Yang, T. Kou, Z. Zhang, Y. Ding, J. Mater. Chem. A. 2, 18229 (2014) https://doi.org/10.1039/C4TA04329D.

[43] N. Raza, T. Kumar, V. Singh, K.-H. Kim, Coord. Chem. Rev. 430, 213660 (2021) https://doi.org/10.1016/j.ccr.2020.213660.

[44] J.Y. Hwang, S.T. Myung, Y.-K. Sun, Chem. Soc. Rev. 46, 3529 (2017) https://doi.org/10.1039/C6CS00776G.

[45] Y. Yang, Y. Xi, J. Li, G. Wei, N.I. Klyui, W. Han, Nanoscale Res. Lett. 12, 394 (2017) https://doi.org/10.1186/s11671-017-2159-9.

[46] B.A. Mei, O. Munteshari, J. Lau, B. Dunn, L. Pilon, J. Phys. Chem. C. 122, 194 (2018) https://doi.org/10.1021/acs.jpcc.7b10582.

[47] Q. Zhou, Y. Li, L. Huang, C. Li, G. Shi, J. Mater. Chem. A. 2, 17489 (2014) https://doi.org/10.1039/C4TA03639E.

[48] H.-P. Cong, X.-C. Ren, P. Wang, S.-H. Yu, Energy Environ. Sci. 6, 1185 (2013) https://doi.org/10.1039/C2EE24203F.

# Figures

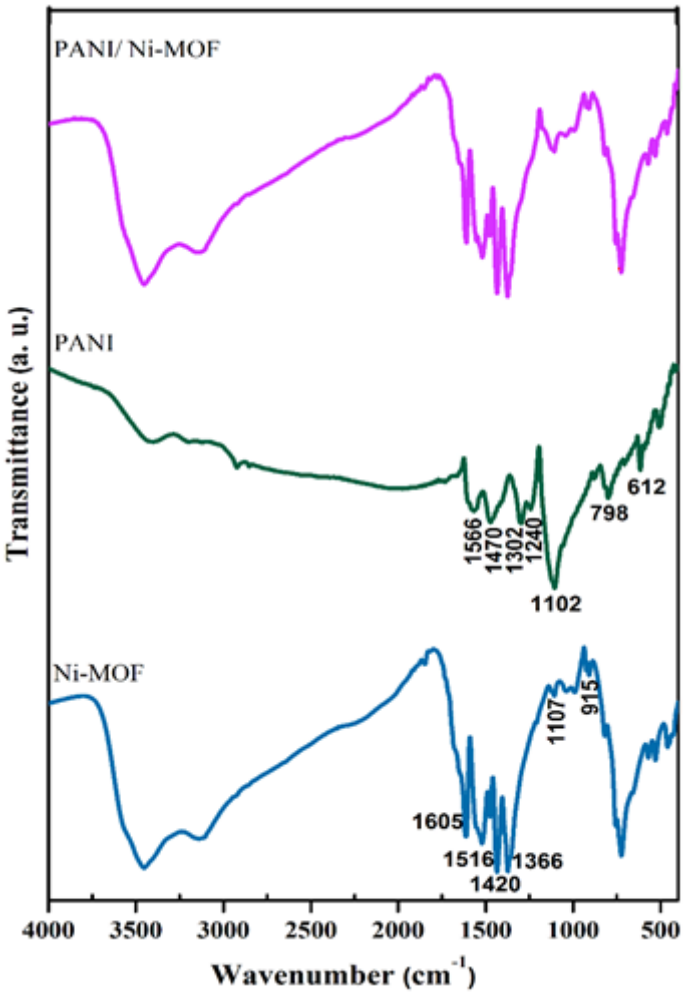


**Figure 1**

The FT-IR spectra of Ni-MOF, PANI, and PANI/Ni-MOF nanocomposite.

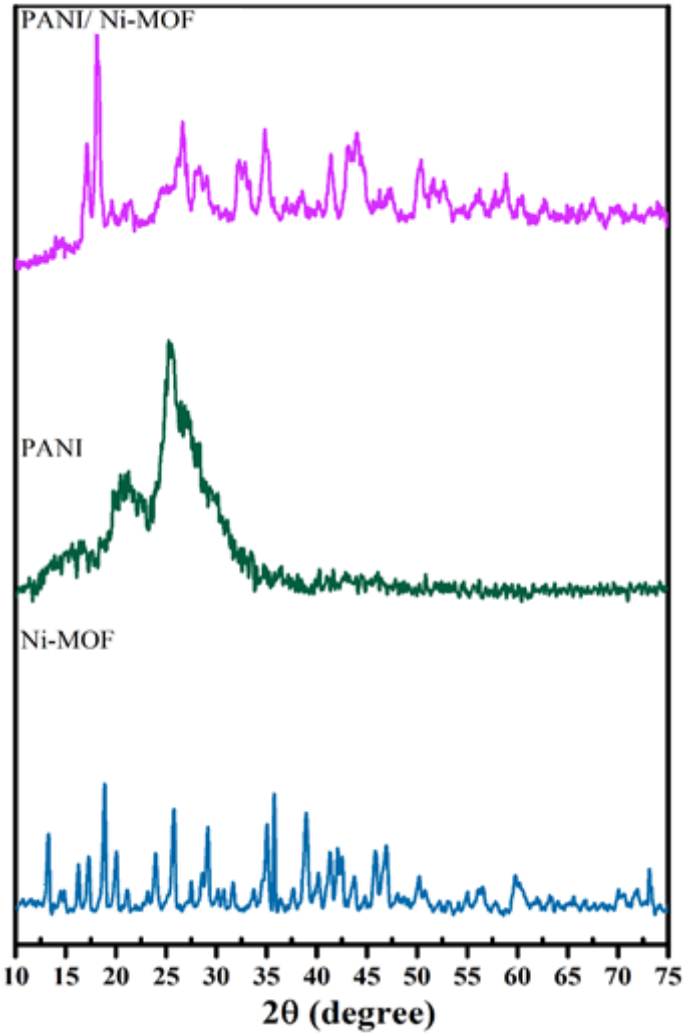


## Figure 2

The powder X-ray diffraction pattern for Ni-MOF, PANI, and PANI/Ni-MOF nanocomposite.

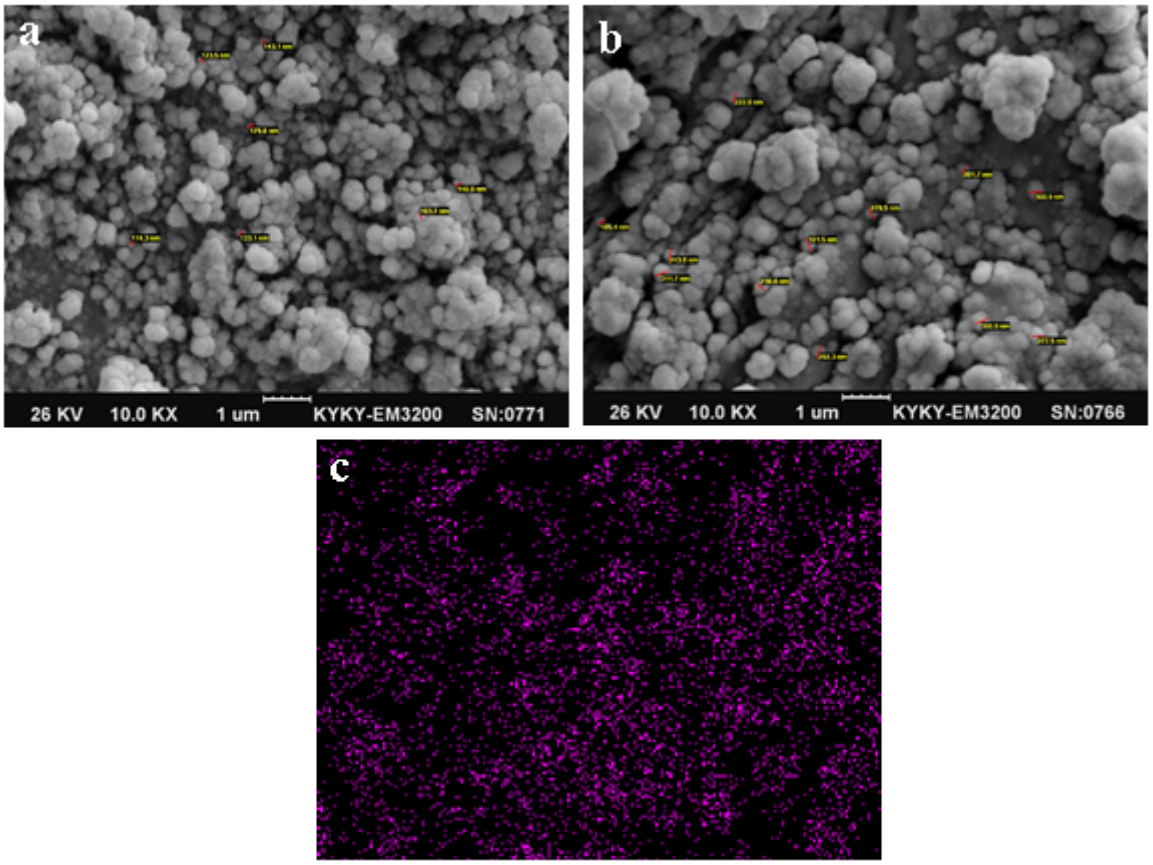


## Figure 3

FESEM image of (a) PANI; FESEM image (b) and Ni elemental mapping (c) of PANI/Ni-MOF naocomposite.

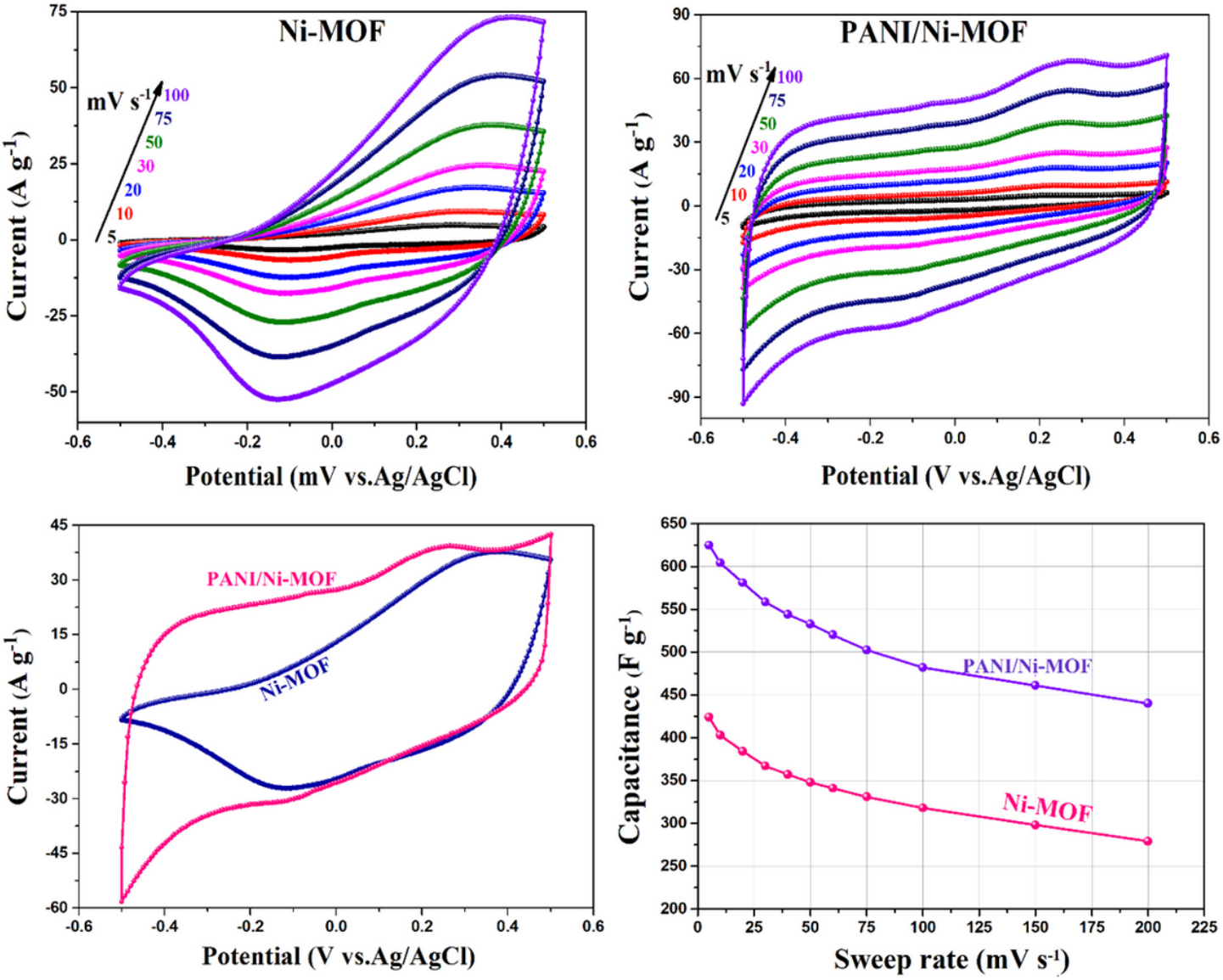


## Figure 4

CV curves of (a) Ni-MOF and (b) PANI/Ni-MOF nanocomposite electrodes at different scan rates, (c) CV curves of Ni-MOF and PANI/Ni-MOF composite electrodes at 50 mV s-1 scan rate in 6 M KOH electrolyte in the potential range from -0.5 to 0.5 V, and (d) alteration of calculated specific capacitance as a function of scan rate.

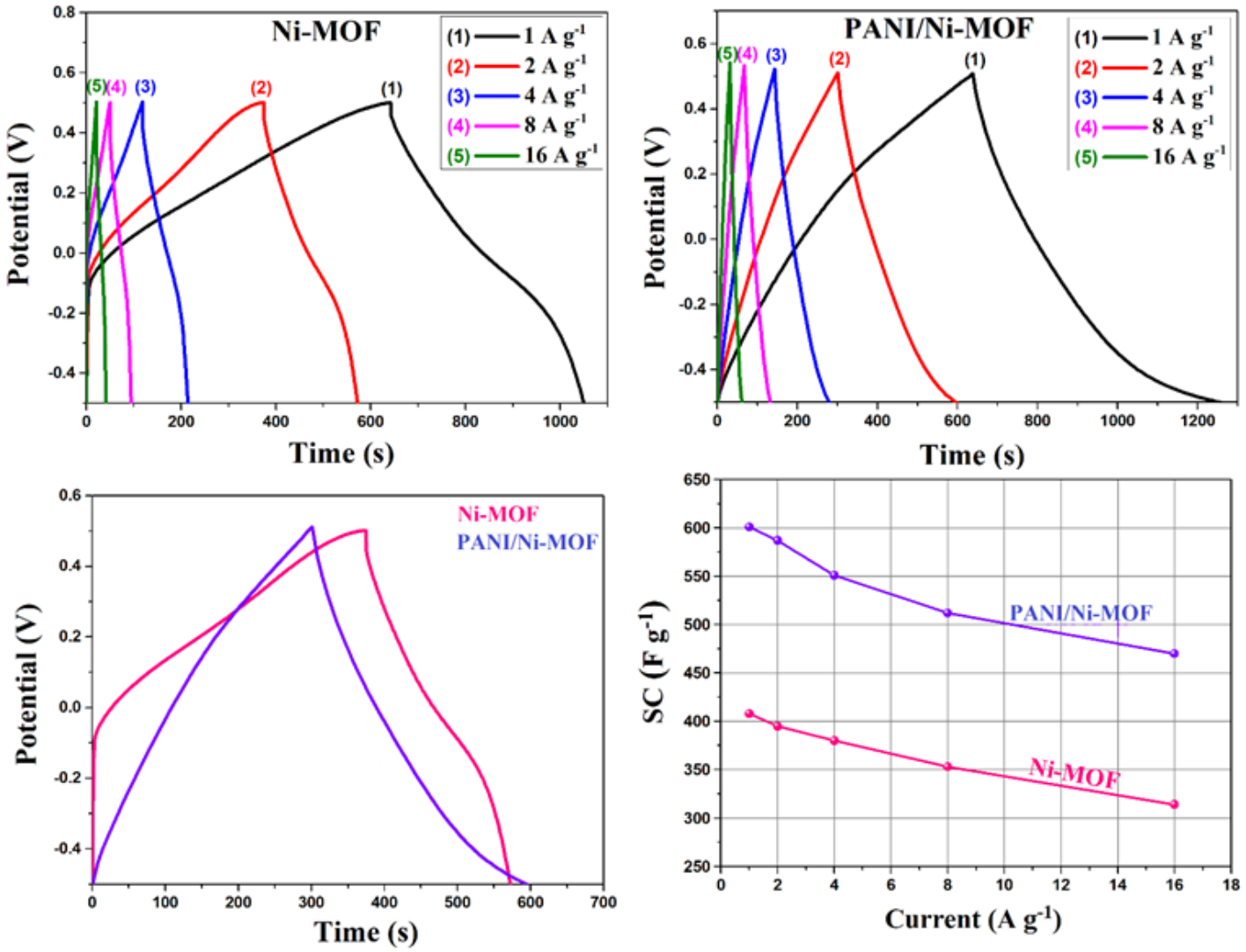


## Figure 5

(a) Galvanostatic charge/discharge curves of Ni-MOF and PANI/Ni-MOF nanocomposite electrodes at various discharge current density, (b) Galvanostatic charge/discharge curves of Ni-MOF and PANI/Ni-MOF nanocomposite electrodes at 2 A g1-, and (c) Alteration of calculated specific capacitance as a function of current density.

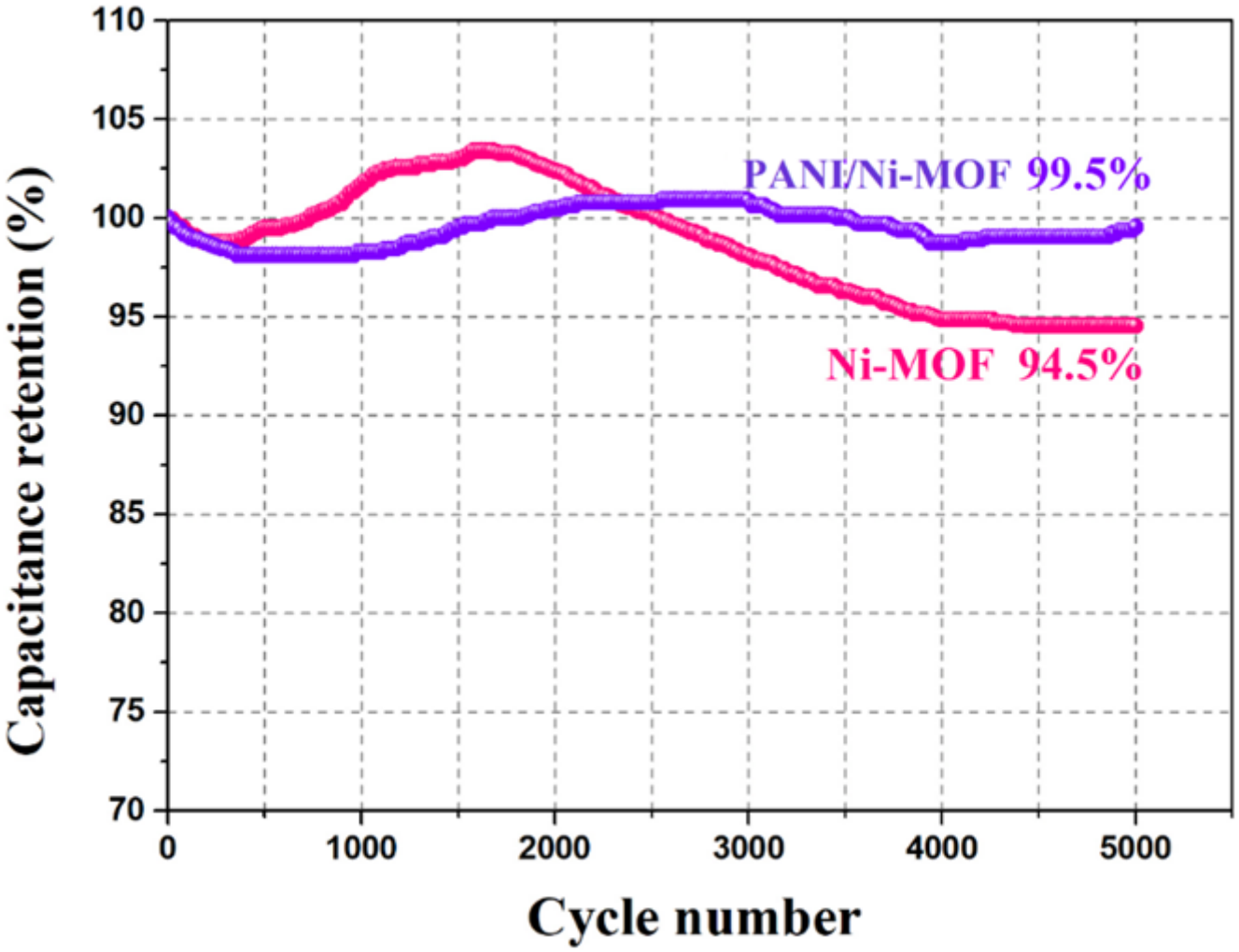


**Figure 6**

Alteration of capacitance retention of Ni-MOF and PANI/Ni-MOF nanocomposite electrodes as a function of cycle number up to 5000 cycles.

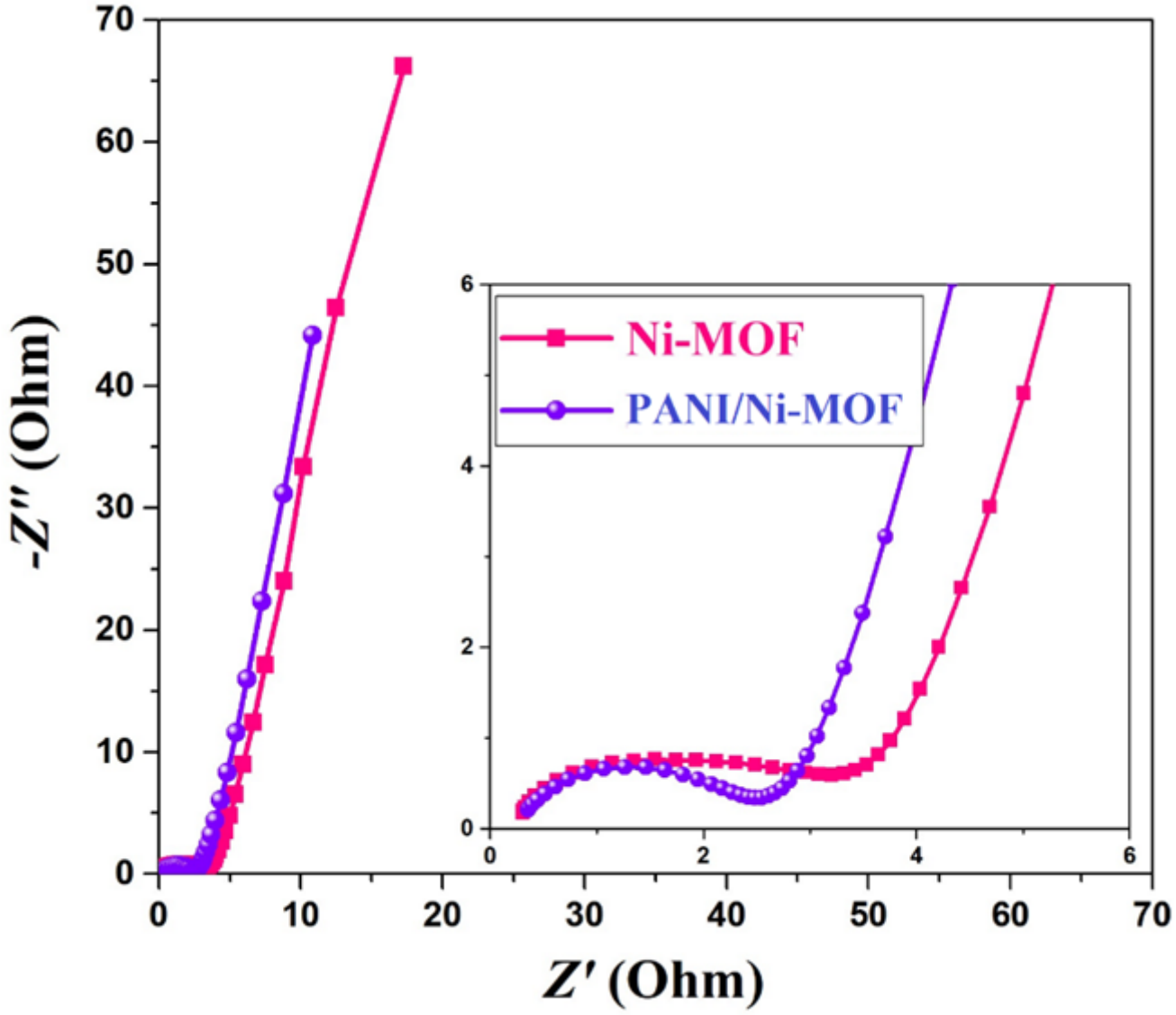


## Figure 7

Nyquist plot of Ni-MOF and PANI/Ni-MOF nanocomposite electrodes.